Improving anti-tumor activity with polymeric micelles entrapping paclitaxel in pulmonary carcinoma

Article *in* Nanoscale · August 2012

DOI: 10.1039/c2nr31517c · Source: PubMed

10 authors, including:

Changyang Gong
Sichuan University
106 PUBLICATIONS **3,750** CITATIONS

SEE PROFILE

Nanoscale

Dynamic Article Links

Cite this: *Nanoscale*, 2012, **4**, 6004

www.rsc.org/nanoscale

PAPER

Improving anti-tumor activity with polymeric micelles entrapping paclitaxel in pulmonary carcinoma

Changyang Gong,*[a] Yongmei Xie,†[a] Qinjie Wu,[a] Yujun Wang,[a] Senyi Deng,[a] Dake Xiong,[a] Lei Liu,[b] Mingli Xiang,*[a] Zhiyong Qian[a] and Yuquan Wei[a]

Received 17th June 2012, Accepted 17th July 2012
DOI: 10.1039/c2nr31517c

Nanoscale polymeric micelles have promising applications as drug delivery systems (DDS). In this work, to improve the anti-tumor activity and eliminate toxicity of the commercial formulation (cremophor EL and ethanol) of paclitaxel (PTX), we developed biodegradable poly(ethylene glycol)-poly(ε-caprolactone) (MPEG-PCL) micelles entrapping PTX by a simple one-step solid dispersion method, which is without any surfactants or additives and is easy to scale up. In addition, the PTX micelles could be lyophilized into powder without any adjuvant and the re-dissolved PTX micelles are stable and homogeneous. The prepared PTX micelles have a mean particle size of 38.06 ± 2.30 nm, a polydispersity index of 0.168 ± 0.014, a drug loading of 14.89 ± 0.06% and an encapsulation efficiency of 99.25 ± 0.38%. A molecular modeling study implied that PTX interacted with PCL as a core, which was embraced by PEG as a shell. The encapsulation of PTX in polymeric micelles enhanced its cytotoxicity by increasing the uptake by LL/2 cells. A sustained *in vitro* release behavior and slow extravasation behavior from blood vessels in a transgenic zebrafish model were observed in the PTX micelles. Furthermore, compared with Taxol®, the PTX micelles were more effective in suppressing tumor growth in the subcutaneous LL/2 tumor model. The PTX micelles also inhibited metastases in the pulmonary metastatic LL/2 tumor model and prolonged survival in both mouse models. Pharmacokinetic and tissue distribution studies showed that after PTX was encapsulated in polymeric micelles, the biodistribution pattern of PTX was altered and the PTX concentration in tumors was increased compared with Taxol® after intravenous injection. In conclusion, we have developed a polymeric micelles entrapping PTX that enhanced cytotoxicity *in vitro* and improved anti-tumor activity *in vivo* with low systemic toxicity on pulmonary carcinoma. The biodegradable MPEG-PCL micelles entrapping PTX may have promising applications in pulmonary carcinoma therapy.

1. Introduction

Cancer is one of the major public health problems in the world, and an increasing number of instances and mortalities of cancer occur every year. Pulmonary carcinoma is one of the leading cancer types and accounts for more than 25% of the total cancer deaths in America.[1] As a conventional treatment of cancer, chemotherapy has proven to be effective and used world-wide in clinics alone or combined with other treatments.[2–5] Although chemotherapy can prolong the survival of cancer patients, it also has severe side effects, such as immune suppression, neurotoxicity and myelosuppression, which dramatically limits the intensity of chemotherapy that can be used and reduces the quality of life of patients.[6] In addition, widespread tissue distribution and rapid elimination of chemotherapeutic agents require a large dosage to keep their therapeutic concentration, which also increases their side effects. To address the challenge, novel delivery strategies should be developed to improve the drug concentration at the tumor site and reduce the side effects.[7]

Water solubility of chemical compounds is a crucial factor for drug development.[8] The poor water solubility of chemotherapeutic agents makes their formulation difficult and therefore limits their clinical applications.[9] Paclitaxel (PTX), a natural anti-microtubule agent from the Pacific yew tree (*Taxus brevifolia*), is effective in treating a variety of solid tumors, such as ovarian cancer, breast cancer, lung cancer, *etc.*[10] PTX is highly hydrophobic (its water solubility is about 1 μg mL^{-1}), therefore cremophor EL and ethanol were employed for its commercial formulation.[11] However, the cremophor EL and ethanol-based formulation is associated with severe side effects including hypersensitivity reactions and peripheral neuropathy, which are

[a]*State Key Laboratory of Biotherapy and Cancer Center, West China Hospital, West China Medical School, Sichuan University, Chengdu, 610041, China. E-mail: chygong14@yahoo.com.cn; xiang_mingli@scu.edu.cn; Fax: +86 86-28-85164060; Tel: +86 86-28-85164063*

[b]*Department of Medical Oncology, Cancer Center, West China Hospital, West China Medical School, Sichuan University, Chengdu, 610041, China*

† Yongmei Xie contributed equally to this work with Changyang Gong, and is the co-first author for this paper.

not well tolerated by some patients.[12,13] Therefore, numerous attempts were made to develop a water-based formulation of PTX, but few have penetrated into clinical practice.

As a fast developing field, nanotechnology has gained increasing attention in drug delivery and cancer therapy.[14–18] Biodegradable polymeric micelles are highlighted as drug delivery systems (DDS) to improve the water solubility and anti-tumor effect of hydrophobic chemotherapeutic agents.[19] Polymeric micelles are usually nanoscale assemblies of amphiphilic polymers, in which hydrophobic blocks form a core serving as a container for the drugs and hydrophilic blocks form a shell that acts as a stabilizing interface.[20] After a hydrophobic drug was encapsulated into polymeric micelles, it could be well dispersed in water to form a homogeneous and stable solution for intravenous administration. In addition, the nano-size and the presence of the hydrophilic shell of micelles prolonged their circulation time *in vivo*. Furthermore, the drug loaded micelles could passively target the tumor site by the enhanced permeability and retention (EPR) effect, therefore improving their anti-tumor effects.[21]

In our previous work, we investigated three different methods (dialysis, freeze-dying, and solid dispersion method) and a series of poly(ethylene glycol)-poly(ε-caprolactone) (MPEG-PCL) copolymers (with different molecular weights or PEG/PCL ratios) for the preparation of PTX micelles.[22] The maximum tolerated dose (MTD) of prepared PTX micelles after a single intravenous injection was also determined, which was 2.6-fold higher than that of Taxol® in mice. In this work, the anti-tumor activity of PTX micelles on pulmonary carcinoma was investigated both *in vitro* and *in vivo*. The solid dispersion method and an MPEG-PCL copolymer with a PEG/PCL ratio of 2000/2000 were used for the preparation of the PTX micelles and a molecular modeling study was conducted to investigate the structure of the PTX micelles. The cytotoxicity and cellular uptake of PTX micelles were studied in detail. The transgenic zebrafish model was used to observe the extravasation behavior of the PTX micelles from blood vessels. Furthermore, the anti-tumor activity of the PTX micelles was evaluated in pulmonary metastatic and subcutaneous LL/2 tumor models. Meanwhile, pharmacokinetic and tissue distribution studies were performed.

2. Materials and methods

2.1 Materials, cell lines and animals

Poly(ethylene glycol) methyl ether (MPEG, Mn = 2000, Fluka, USA), ε-caprolactone (ε-CL, Alfa Aesar, USA), stannous octoate ($Sn(Oct)_2$, Sigma, USA), Roswell Park Memorial Institute 1640 medium (RPMI 1640, Gibco, USA), Dulbecco's modified Eagle's medium (DMEM, Sigma, USA), 3-(4,5-dimethyl-2-thiazolyl)-2,5-diphenyl-2*H*-tetrazolium bromide (methyl thiazolyl tetrazolium, MTT, Sigma, USA), fluorescein isothiocyanate (FITC, Sigma, USA), 4′,6-diamidino-2-phenylindole 2hci (DAPI, Sigma, USA), Taxol® (Bristol-Myers Squibb, USP), paclitaxel (Sigma, USA) and acetonitrile (HPLC grade, Fisher Scientific, UK) were used without further purification. All the materials used in this article were analytic reagent (AR) grade and used as received.

L929 cells and LL/2 cells were purchased from the American Type Culture Collection (ATCC; Rockville, MD), which grew in RPMI 1640 or DMEM supplement with 10% fetal bovine serum (FBS), respectively. The cell cultures were maintained in a 37 °C incubator with a humidified 5% CO_2 atmosphere.

C57BL/6 mice, weighing 18 ± 2 g, were used for *in vivo* anti-tumor tests and pharmacokinetic studies. The animals were purchased from the Laboratory Animal Center of Sichuan University and were housed at a controlled temperature of 20–22 °C, relative humidity of 50–60% and with 12 h light–dark cycles. The animals were provided with standard laboratory chow and tap water *ad libitum*. All the animals were quarantined for a week before treatment. All the animal procedures were performed following the protocol approved by the Institutional Animal Care and Treatment Committee of Sichuan University (Chengdu, P.R. China). All the mice were treated humanely throughout the experimental period.

2.2 Synthesis of the MPEG-PCL copolymer and FITC labeled PTX (FITC-PTX)

The MPEG-PCL copolymer was prepared by ring-opening polymerization of ε-CL initiated by MPEG using $Sn(Oct)_2$ as the catalyst, which was reported in previous contributions.[23–25] Briefly, the calculated amount of MPEG and ε-CL were introduced into a dry glass ampoule under a nitrogen atmosphere and a certain amount of $Sn(Oct)_2$ was added into the reaction vessel under mild agitation. The reaction system was kept at 130 °C for 6 hours. The purified MPEG-PCL copolymer was kept in desiccators before further use. The obtained MPEG-PCL copolymer was characterized by ^{1}H nuclear magnetic resonance spectroscopy (^{1}H-NMR, Varian 400 spectrometer, Varian, USA), Fourier transform infrared spectroscopy (FTIR, NICOLET 200SXV, Nicolet, USA), and gel permeation chromatography (GPC, Agilent 110 HPLC, USA).

FITC-PTX was synthesized according to Fig. 1. Compound **3** was synthesized according to a literature method with some modifications.[26] Briefly, *N*-benzyloxycarbonyl-6-aminohexanoic acid (**2**) (185.7 mg, 0.7 mmol) and dicyclohexylcarbodiimide (144.4 mg, 0.7 mmol) were added to a solution of PTX (170.8 mg, 0.2 mmol) (compound **1**, Sigma, USA) in anhydrous acetonitrile (30 mL). The reaction mixture was stirred at room temperature for 48 h. The solvent was evaporated and the residue was purified with column chromatography (ethyl acetate : petroleum ether = 1 : 1) to give compound **3** (164.3 mg, 74.6%). ^{1}H-NMR ($CDCl_3$) δ: 8.14 (d, J = 7.6, 2H), 7.74 (d, J = 7.2, 2H), 7.64–7.60 (m, 1H), 7.54–7.48 (m, 3H), 7.44–7.31 (m, 13H), 6.99 (d, J = 9.2, 1H), 6.30–6.23 (m, 2H), 5.99–5.96 (m, 1H), 5.69 (d, J = 6.8, 1H), 5.51 (d, J = 3.6, 1H), 5.06 (s, 1H), 4.98 (d, J = 8.0, 1H), 4.80–4.76 (m, 1H), 4.48–4.44 (m, 1H), 4.33–4.20 (m, 2H), 3.82 (d, J = 7.2, 1H), 3.20–3.09 (m, 3H), 2.62–2.53 (m, 2H), 2.46 (s, 3H), 2.42–2.27 (m, 3H), 2.23 (s, 3H), 2.18–2.12 (m, 1H), 1.95 (s, 3H), 1.69 (s, 3H), 1.66–1.59 (m, 2H), 1.53–1.42 (m, 2H), 1.36–1.26 (m, 3H), 1.23 (s, 3H), 1.14 (s, 3H).

Compound **3** (110 mg, 0.1 mmol) was dissolved in MeOH (5 mL) and formic acid (0.35 mL). 10% Pd/C (10 mg) was then added and the reaction mixture was stirred at room temperature for 24 h. The resulting mixture was filtered and concentrated

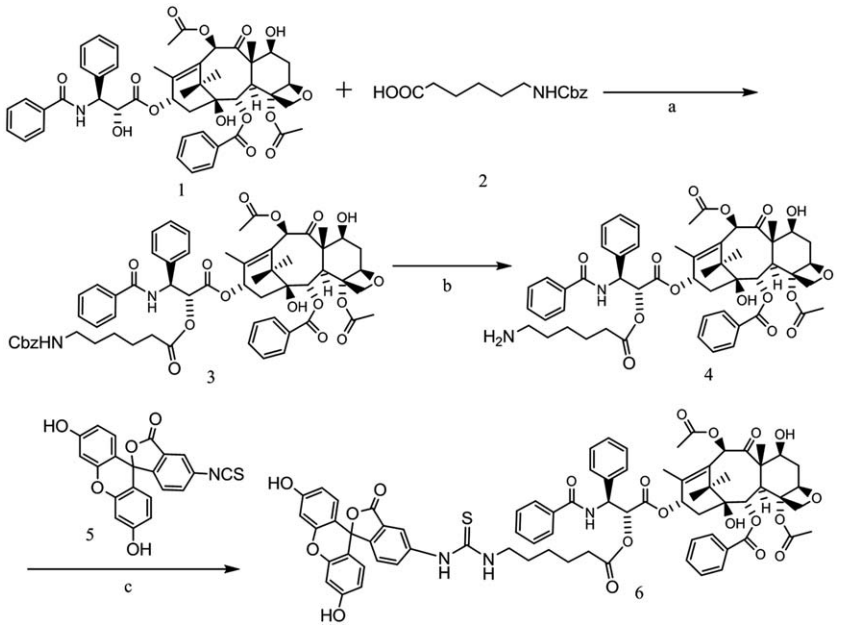

Fig. 1 Synthetic route of FITC labeled PTX (FITC-PTX). Reagents and conditions: (a) DCC, acetonitrile, 48 h, rt; (b) MeOH, formic acid, Pd/C, 24 h, rt; (c) DMF, TEA, 4 h, rt.

under vacuum to give compound **4** (82.4 mg, 85.2%) which was then used immediately for the synthesis of compound **6**.

Compound **4** (70 mg, 0.07 mmol) in DMF (2 mL) was added to FITC (27.3 mg, 0.07 mmol) and triethylamine (10 μl, 0.07 mmol). The reaction mixture was stirred for 4 h at room temperature and then concentrated under reduced pressure. The residue was purified by column chromatography on silica gel with CH_2Cl_2–MeOH (95 : 5) to give compound **6** (49.2 mg, 51.8%) as a yellow solid.

2.3 Preparation and characterization of the PTX micelles

The PTX micelles were prepared by a one-step solid dispersion method. Briefly, 100 mg of PTX and MPEG-PCL copolymer with different ratios were co-dissolved in 5 mL of dehydrated alcohol under mild stirring. Then, the solution was evaporated in a rotary evaporator at 60 °C. During this process, homogenous co-evaporation was obtained, and PTX was distributed in MPEG-PCL copolymer as an amorphous substance. Subsequently, the co-evaporation was dissolved in normal saline (NS) at 60 °C to self-assemble into micelles with PTX encapsulated within. The PTX micelles were filtered through a 0.22 μm syringe filter (Millex-LG, Millipore Co., USA), and were lyophilized and stored at 4 °C before use.

The concentration of PTX was determined by a high performance liquid chromatography (HPLC, Shimadzu LC-20AD, Japan) instrument and the sample was diluted before measurement. The solvent delivery system was equipped with a column oven (CTO-20A) and a plus autosampler (SIL-20AC). Detection was taken on a diode array detector (SPD-M20A). Chromatographic separations were performed on a reversed phase C_{18} column (4.6 mm × 150 mm, 5 μm, zorbax eclipse XDB, Agilent, USA) and the column temperature was kept at 30 °C. Acetonitrile/water (43/57, v/v) was used as the eluent at a flow rate of 1 mL min^{-1}. The detection wavelength was 227 nm.

The drug loading (DL) and encapsulation efficiency (EE) of the PTX micelles were determined as follows. Briefly, 10 mg of lyophilized PTX micelles were dissolved in 0.1 mL of acetonitrile. The amount of PTX in the solution was determined by HPLC. The DL and EE of PTX micelles were calculated according to eqn (1) and (2):

$$\mathrm{DL} = \frac{\text{Drug}}{\text{Polymer} + \text{drug}} \times 100\% \quad (1)$$

$$\mathrm{EE} = \frac{\text{Experimental drug loading}}{\text{Theoretical drug loading}} \times 100\% \quad (2)$$

The particle size distribution and zeta potential of the prepared PTX micelles were determined by dynamic light scattering (DLS, Malvern Nano-ZS 90 laser particle size analyzer) at 25 °C. All the results were the mean of three test runs, and all data were expressed as the mean ± standard deviation (SD).

The morphological characteristics of the PTX micelles were examined by transmission electron microscopy (TEM, H-6009IV, Hitachi, Japan). The PTX micelles were diluted with distilled water and placed on a copper grid covered with nitrocellulose. The samples were negatively stained with phosphotungstic acid and dried at room temperature.

2.4 Molecular modeling study

It is hard to experimentally determine the structures of PCL, PEG and MPEG-PCL copolymer at the atomic level. Consequently, we constructed these structures by the aid of a molecular mechanics (MM) method and a molecular dynamics (MD) approach. Initially, PCL ($n = 18$), PEG ($n = 45$) and MPEG-PCL were built by employing the HyperChem software.[27] Then the structures experienced a series of geometry optimizations at the MM level with the OPLS method[28] using a steepest descent algorithm and a Flether–Rooves algorithm.[29] They were optimised until the root

mean square gradient was less than 0.05 kcal mol^{-1} $Å^{-1}$). Finally, simulated annealing was performed on the optimized structures by using MD so as to obtain a lower energy minimum. The solvent effect was considered implicitly by CHARMM27 in the process of the MD simulation.[30] The MD simulations include heating from 0 K to 600 K, simulating at 600 K, cooling from 600 K to 300 K, and running at 300 K. At each stage, the simulated time is set to 100 picoseconds.

2.5 Cytotoxicity of the MPEG-PCL copolymer and PTX micelles

Cytotoxicity tests of PTX micelles and free PTX were preformed on LL/2 cells. The LL/2 cells were plated at a density of 1×10^4 cells per well in 100 μL of medium in 96-well plates and grown for 48 hours. The cells were then exposed to a series of PTX micelles at different concentrations for 48 hours. Then, the viability of cells was measured using the MTT method. Briefly, the mean percentage of cell survival relative to that of untreated cells was estimated from the data of six individual experiments, and all data were expressed as the mean ± SD. In addition, a cytotoxicity evaluation of the MPEG-PCL copolymer was conducted on LL/2 cells and L929 cells using the MTT method presented above.

2.6 Cellular uptake of PTX micelles

To measure the uptake of PTX into cells by confocal microscopy and flow cytometric (FCM) analysis, FITC-PTX was used. LL/2 cells at log phase were seeded onto acid etched glass coverslips at a density of 2×10^5 cells per well and cultured in 1 mL of growth medium. After being incubated for 24 hours, the growth medium was removed, and the cells were exposed to a serum-free medium containing blank micelles, free FITC-PTX, or FITC-PTX micelles at a final PTX concentration of 2 μg mL^{-1}, respectively. After incubation at 37 °C for 0, 2 and 4 hours, the media were removed and carefully washed with PBS. For studies by confocal microscopy, the cells were fixed with cold acetone, washed again with PBS, stained with DAPI, and imaged using a confocal microscope (DM6000 CS, Leica, Germany). Each experiment was performed in triplicate. For FCM analysis, cells were collected and washed with PBS. Then, intracellular FITC-PTX fluorescence was analyzed by FCM after excitation with a 488 nm argon laser using a BD FACSCalibur (BD, USA). The fluorescence emissions at 520 to 530 nm from 10 000 cells were collected, amplified and scaled to generate a single parameter histogram.

For the quantification of the *in vitro* cellular uptake of the PTX micelles by LL/2 cells, the cells were seeded on 24-well plates with a density of 2×10^5 cells per well and cultured in 1 mL of growth medium. After being incubated for 24 hours, the growth media were removed and the cells were exposed to a serum-free medium containing blank micelles, Taxol®, or PTX micelles at a final PTX concentration of 4 μg mL^{-1}, respectively. After incubation for 0, 2, and 4 hours, the cells were lysed and PTX was extracted by a mixture of ethyl acetate and *n*-hexane (1 : 3) and measured by HPLC (Shimadzu LC-20AD, Japan).

2.7 *In vitro* drug release study

A modified dialysis method was employed to investigate the *in vitro* release behavior of PTX from free PTX and PTX micelles. Briefly, 200 μL of free PTX or PTX micelles were placed in dialysis bags (molecular mass cutoff is 3.0 kDa and the dialysis area is 1 cm^2). The dialysis bags were incubated in 10 mL of PBS (pre-warmed to 37 °C, pH = 7.4) containing Tween80 (0.5% wt) at 37 °C with gentle shaking (100 rpm). At specific time points, all the release media were removed and replaced by pre-warmed fresh release media. After centrifugation for 10 min, the supernatants of the removed release media were collected and stored at −20 °C until analysis. The released PTX samples were quantified using HPLC. All the results were the mean of three test runs, and all data were expressed as the mean ± SD.

2.8 *In vivo* drug extravasation study in the transgenic zebrafish model

Due to the absence of fluorescence in PTX, FITC labeled PTX (FITC-PTX) was synthesized and used in a drug extravasation study *in vivo*. The zebrafish model has been widely used for drug evaluation.[31,32] In this study, extravasation of free FITC-PTX and FITC-PTX micelles was investigated in FLK-1 promoter mCherry transgenic (Tg(FLK-1:mCherry)) zebrafish line (provided by Shuo Lin, UCLA, Los Angeles, CA). The endothelial cells of Tg(FLK-1:mCherry) zebrafish had red fluorescence, thus the bright and consistent fluorescence of blood vessels in the zebrafish suggested they could provide an ideal tool for testing the blood vessel extravasation of drugs. Tg(FLK-1:mCherry) zebrafish was raised by standard methods as described, and embryos were treated with 1-phenyl-2-thiourea (PTU) and maintained at 28 °C in a Holtfreter's solution after transplantation procedures.[33] Fourteen eight-cell post-fertilization (hpf) embryos were stripped off the egg sheath. Subsequently, the zebrafish were anesthetized with 0.01% tricaine, and free FITC-PTX (1 mg mL^{-1}) or FITC-PTX micelles (1 mg mL^{-1}) were injected into the zebrafish embryo circulation (twenty zebrafish per group) through the perivitelline space using a Cell Tram Vario injector (Eppendorf, USA) equipped with a glass micropipette ($L = 50$ mm, diameter of the needle opening is about 25 μm). A Zeiss Stemi 2000-C dissecting microscope (Carl Zeiss Microimaging Inc., Thornwood, NY) was used during the injections. At specific time, the transgenic zebrafish were examined under a confocal microscope (DM6000 CS, Leica, Germany). The red florescence of the zebrafish endothelial cells was examined to determine the sites of blood vessels. The FITC channel was used to examine FITC-PTX-derived green florescence.

2.9 *In vivo* tumor models and treatment plans

In the pulmonary metastatic LL/2 model, mice were intravenously injected with 0.1 mL of cell suspension containing 2×10^5 LL/2 cells on day 0. On day 5, the tumor bearing mice were randomized into 4 groups (12 mice per group). At days 5, 8, and 11, the mice were intravenously injected with NS (control), blank micelles, Taxol® (4 mg per kg body weight) or PTX micelles (4 mg per kg body weight), respectively. For the tumor growth inhibition study (6 mice per group), the mice were scarified by cervical vertebra dislocation at day 21. After day 21, the mice in the NS group began to die. The lungs in each group were immediately harvested and weighed, and the number of tumor

nodules was counted in each lung. To further study the therapeutic effect of PTX micelles in the pulmonary metastatic LL/2 model, the survival times of the mice were recorded (6 mice per group).

In the subcutaneous LL/2 model, the mice were subcutaneously injected with 0.1 mL of LL/2 cell suspension containing 5×10^5 cells in the right flank at day 0. When the tumors were palpable (day 6), the tumor bearing mice were randomized into four groups (12 mice per group). At days 6, 9 and 12, the mice were intravenously injected with NS (control), blank micelles, Taxol® (4 mg per kg body weight) or PTX micelles (4 mg per kg body weight), respectively. For the tumor growth inhibition study (6 mice per group), the tumor size was measured every two days using callipers. The tumor volume was calculated using the equation $vol = (a \times b^2)/2$, where *vol* is tumor volume, *a* is the length of the major axis, and *b* is the length of the minor axis. On day 27, the mice in the control group began to die, and the other mice were scarified by cervical vertebra dislocation. Subsequently, the tumors in each group were immediately harvested and analyzed. To further study the therapeutic effect of PTX micelles in subcutaneous LL/2 model, the survival times of the mice were recorded (6 mice per group).

2.10 Quantitative assessment of apoptosis

The tumor tissues in the subcutaneous LL/2 model were harvested, fixed in 4%wt paraformaldehyde (PFA), embedded in paraffin, and sectioned. Terminal deoxynucleotidyl transferase-mediated nick-end labeling (TUNEL) staining was done using an *in situ* cell death detection kit (DeadEnd™ Fluorometric TUNEL System, Promega, Madison, USA) following the manufacturer's protocol, which is based on the enzymatic addition of digoxigenin-nucleotide to the nicked DNA by recombinant terminal deoxynucleotidyl transferase (rTdT).[34] In the tumor tissue sections, four equal-sized fields were randomly chosen and analyzed. The apoptotic index was calculated as a ratio of the apoptotic cell number to the total tumor cell number in each high-power field.

2.11 Immunohistochemical determination of Ki-67

Paraffin embedded tumor tissue was sliced into sections for Ki-67 staining using the labeled streptavidin–biotin method.[35] The primary antibody was rat anti-mouse monoclonal antibody Ki-67 (Gene Tech) and the secondary antibody was biotinylated goat anti-rat immunoglobulin (BD Biosciences Pharmingen). To quantify Ki-67 expression, the Ki-67 labelling index (Ki-67 LI) was calculated as the number of Ki-67-positive cells/total number of cells counted under ×400 magnification in five randomly selected areas in each tumor sample by two independent investigators in a blind study.

2.12 Pharmacokinetic and tissue distribution studies

Pharmacokinetics and tissue distribution studies of PTX micelles were performed in male C57BL/6 mice. The mice were subcutaneously injected with 0.1 mL of LL/2 cell suspension containing 5×10^5 cells in the right flank. When the volume of the tumors was approximately 200 mm^3, the mice were randomized into two groups (45 mice per group), which were injected intravenously with Taxol® (4 mg per kg body weight) or PTX micelles (4 mg per kg body weight), respectively. At specific time points, five mice in each group were scarified and blood samples and tissue samples (heart, lungs, liver, spleen, kidney and tumor) were collected. For the pharmacokinetic study, plasma were obtained immediately and stored at −20 °C until analyzed by HPLC. The pharmacokinetic parameters of PTX after intravenous administration were calculated using a non-compartmental model by the Drug and Statistics (DAS) software (version 2.1.1, Mathematical Pharmacology Professional Committee, China). For tissue distribution studies, tissue samples were weighted and stored at −20 °C until analyzed by HPLC. The tissue distribution was expressed as the amount of PTX per gram of the tissues.

2.13 Statistical analysis

The statistic analysis was carried out using the SPSS 15.0 software (Chicago, IL, USA). Comparisons of tumor volume, tumor nodules number and lung weight were performed using one-way analysis of variance (ANOVA). Survival curves were generated based on the Kaplan–Meier method and the statistical significance was determined by Mann–Whitney *U*-tests. A P value <0.05 on a 2-tailed test was considered statistically significant.

3. Results

3.1 Preparation and characterization of PTX micelles

The biodegradable MPEG-PCL copolymer was successfully synthesized by ring-opening polymerization of ε-CL on MPEG. The molecular weight of the prepared MPEG-PCL diblock copolymer determined by ^{1}H-NMR was 3950 (PEG/PCL ratio: 2000/1950).

As shown in Fig. 2A, PTX micelles were prepared by a one-step solid dispersion method, which is easy to produce and scale up. During the evaporation process, PTX was distributed in MPEG-PCL copolymer as an amorphous substance. Subsequently, the co-evaporation was dissolved in NS to self-assemble into the PTX micelles. When the in-feed mass ratio of PTX/MPEG-PCL copolymer was 15/85, the average particle size of the prepared PTX micelles was 38.06 ± 2.30 nm with a polydispersity index (PDI) of 0.168 ± 0.014 and a zeta potential of −1.21 ± 0.44 mV (Fig. 2C). According to the particle size distribution spectrum shown in Fig. 2B, the PTX micelles had a very narrow particle size distribution. Furthermore, the DL and EE of the obtained PTX micelles were 14.89% ± 0.06% and 99.25% ± 0.38%, respectively. The TEM image of the PTX micelles is shown in Fig. 2D, which reveals that the PTX micelles are spherical in aqueous solution. The diameter of the PTX micelles observed by TEM was in good agreement with the results of the DLS, which demonstrates that the prepared PTX micelles are stable and could be well-dispersed in aqueous solution. The appearance of the prepared PTX micelles is presented in Fig. 2E. A clear solution of blank micelles (Fig. 2E(b)) and PTX micelles (Fig. 2E(c)) could be observed. In addition, the PTX micelles can be lyophilized into a power form without any adjuvants (Fig. 2E(e)), and the re-dissolved PTX micelles are stable and homogeneous (Fig. 2E(g)).

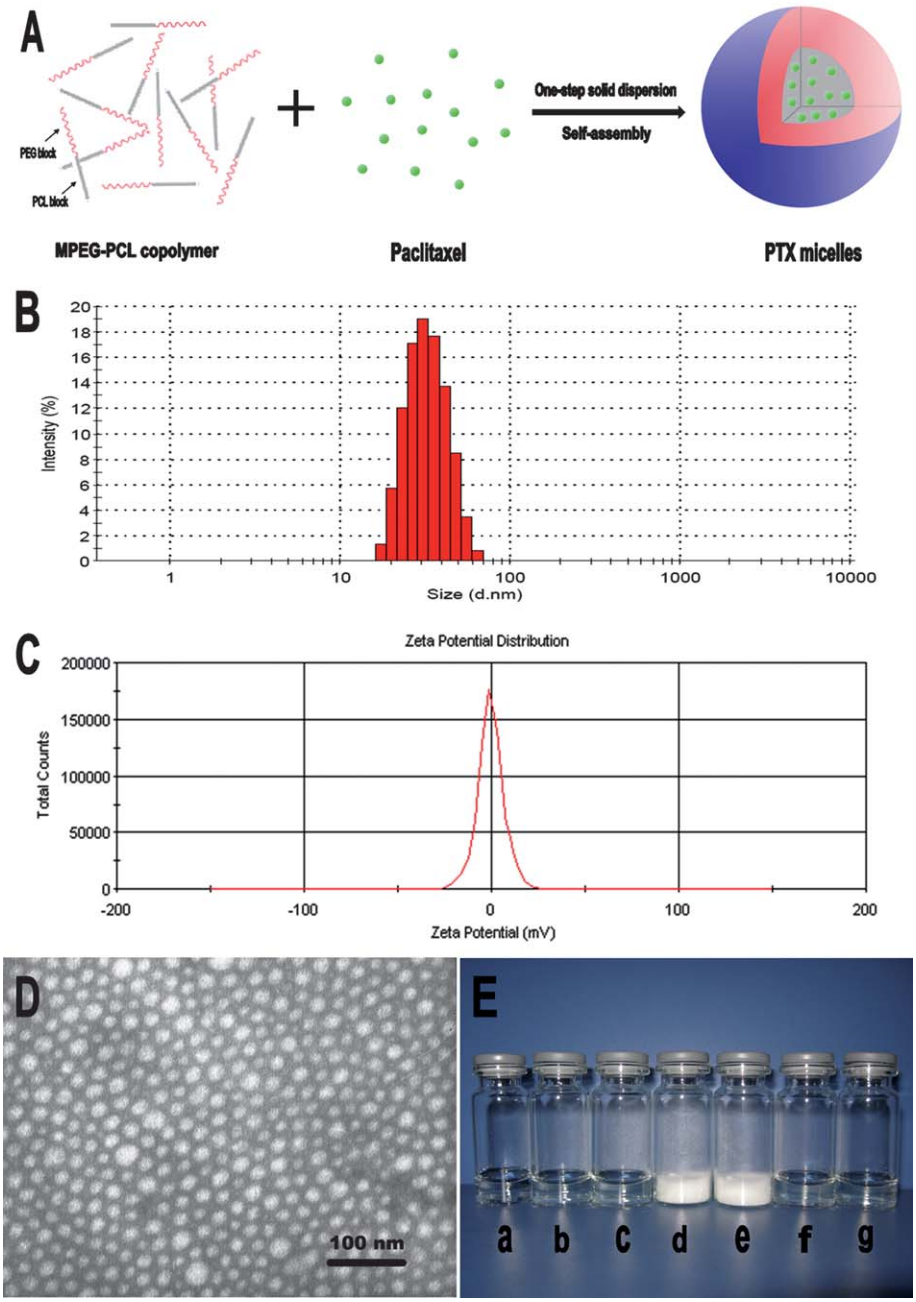

Fig. 2 Preparation and characterization of the PTX micelles. (A) Preparation scheme of the PTX micelles by self-assembly of the MPEG-PCL copolymer and PTX; (B) particle size distribution of the PTX micelles; (C) zeta potential of the PTX micelles; (D) TEM image of the PTX micelles; (E) morphology of (a) water, (b) blank micelles, (c) the PTX-micelles, (d) a freeze-dried powder of blank micelles, (e) a freeze-dried powder of PTX micelles, (f) re-dispersed freeze-dried blank micelles and (g) re-dispersed freeze-dried PTX micelles.

3.2 Molecular modeling study

The structures of the simulated polymers are shown in Fig. 3A–C. Docking experiments were conducted to explore the recognition of polymers PEG, PCL and MPEG-PCL for PTX by employing AutoDock Vina.[36] The binding affinity between PCL and PTX is -9.62 kJ mol^{-1}. It seems that PTX cannot find a proper place to dwell on the surface of PEG because the binding affinity value is zero. Interestingly, there exists a binding affinity between MPEG-PCL and PTX. The binding affinity is -5.85 kJ mol^{-1}. The suggested conformation of the complex composed of PCL and PTX was obtained by using AutoDock Vina and is shown in Fig. 3D and E.

As shown in Fig. 3F and G, the structure of the MPEG-PCL copolymer is shown with a solid surface and colored differently. The surface area has been calculated with the Hyperchem software.[27] The surface area of the PEG moiety is 1423.08 Å^2 and that of the PCL part is 1308.15 Å^2. As can be seen in Fig. 3G, there is a tendency for much of the PEG to be exposed to the solvent. This not difficult to understand: since in the PEG part,

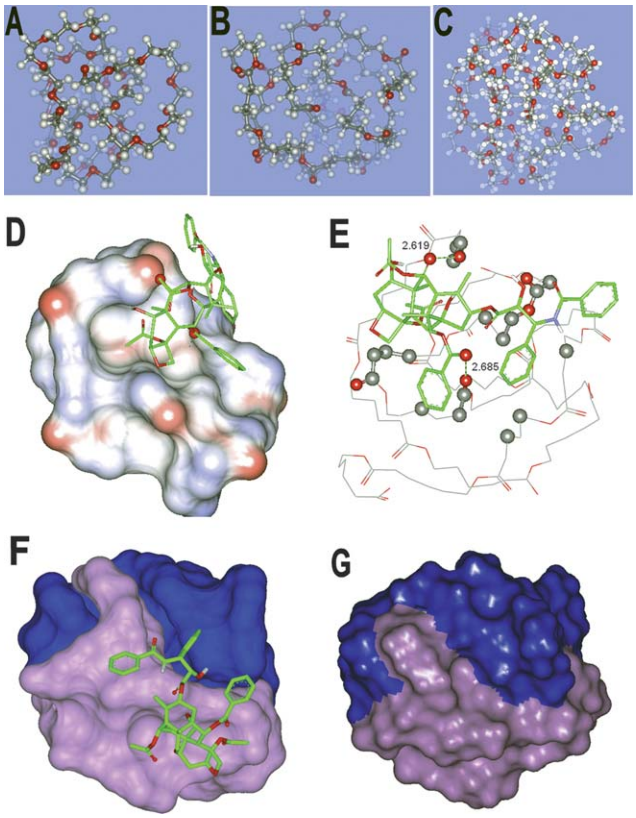

Fig. 3 Molecular modeling study of MPEG-PCL copolymer and PTX. Simulated structures of (A) PEG, (B) PCL and (c) the MPEG-PCL copolymer are shown. (D) and (E) present the conformation of the complex consisting of PCL and PTX (atom coloring: green, carbon; red, oxygen; blue, nitrogen; white, hydrogen). Non polar hydrogen atoms are hidden for the sake of clarity. Atoms of PCL that interact with PTX are highlighted with balls and PTX is sketched with sticks. Atoms that form an H-bond with PCL are drawn with balls. (F) and (G) show the conformation of the MPEG-PCL polymer complexed with PTX and the polymer alone, respectively. PTX is depicted with sticks and the polymer is represented by the solid surface method. The PEG moiety is blue, while the PCL part is pink.

the number of polar atoms is higher than in PCL, PEG shows a preference for exposure to a polar environment and interacts with water molecules.

Combining the docking results with the experimental data, it is reasonable to speculate that PTX interacts with one or more of the PCL parts of MPEG-PCL and that PCL is embraced by PEG.

3.3 Cytotoxicity and cellular uptake of PTX micelles

The cytotoxicity of blank MPEG-PCL micelles was evaluated by a cell viability assay using LL/2 and L929 cells for 48 hours, respectively. In Fig. 4A, with an increase in the concentration of the MPEG-PCL micelles, the viability of LL/2 and L929 cells decreased accordingly. When the input concentration of micelles was 1000 mg mL^{-1}, the cell viabilities were higher than 90.66% or 86.62% for LL/2 or L929 cells, respectively. The cytotoxicity studies suggested that the MPEG-PCL micelles were biocompatible with very low cytotoxicity. Therefore, MPEG-PCL micelles could be regarded as a safe drug delivery carrier.

To compare the cytotoxic activity of the PTX micelles with free PTX, LL/2 cells were exposed to a series of equivalent concentrations of PTX micelles or free PTX for 48 hours, and the viability of the cells was quantified using the MTT method. Fig. 4B shows that both free PTX and the PTX micelles significantly inhibited the growth of LL/2 cells in a dose-dependent manner. The half maximal inhibitory concentration (IC50) of the PTX micelles was much lower than that of free PTX (mean = 21.31 *versus* 32.11 mg mL^{-1}, $P < 0.01$, ANOVA). The results indicate that encapsulation of PTX in MPEG-PCL micelles enhances the cytotoxic activity of PTX.

To investigate the mechanism of the enhanced cytotoxic activity of the PTX micelles, cellular uptake tests of the PTX micelles were conducted using FITC-PTX. FITC-PTX was synthesized as described above. Cellular uptake studies of FITC-PTX micelles were conducted by visualizing the intrinsic green fluorescence of FITC-PTX using confocal microscopy. Fig. 5A presents the images of cells treated with blank micelles as control, free FITC-PTX and FITC-PTX micelles at 0, 2, and 4 h, respectively. Cells in control group did not show any fluorescence at any time. For free FITC-PTX, a very slight fluorescence was observed at 2 h after incubation and green fluorescence was enhanced after 4 h incubation. In the FITC-PTX micelles group, FITC-PTX micelles could rapidly accumulate in the cytosol over a 2 h incubation, which showed a bright green fluorescence and a brighter green fluorescence was observed after 4 h. Furthermore, an FCM analysis was also used to determine the cellular uptake of free FITC-PTX and FITC-PTX micelles. Flow cytometric histograms (Fig. 5B) showed that uptake of FITC-PTX micelles in cells is much more compared with free FITC-PTX after 4 h incubation.

To quantitatively determine the cellular uptake of PTX, LL/2 cells were exposed to free PTX or PTX micelles at different time intervals. Then, the cells were lysed and PTX was extracted and measured by HPLC. In Fig. 5C, the PTX micelles-treated cells showed 0.57 μg more PTX accumulated in the cells within 2 h than cells treated with free PTX and the PTX micelles treatment continued to gradually increase cellular PTX levels over longer times. These results suggest that encapsulation of PTX into MPEG-PCL micelles enhances the delivery of PTX into cells to increase the cytotoxic efficacy of the drug.

3.4 *In vitro* drug release and *in vivo* drug extravasation studies

Fig. 6A shows the *in vitro* release profiles of free PTX and PTX micelles in PBS. In comparison with the fast release profile of free PTX, the cumulative release rate of PTX from the PTX micelles is much slower, followed by a sustained release for up to 2 weeks. In the first 48 hours, approximately 90% of PTX was released into the outside media in free PTX, whereas only 35% of PTX was released from the PTX micelles. The cumulative release rate of PTX micelles was 68.50 ± 6.46%, which was much lower than that of free PTX (94.10 ± 2.07%, $P < 0.001$). This controlled release of PTX from the PTX micelles indicates their potential applicability as a drug delivery system to minimize the exposure of healthy tissues while increasing the accumulation of the therapeutic drug in the tumor site.

Blood vessel extravasation behaviors of free FITC-PTX or FITC-PTX micelles were investigated in the Tg(FLK-1:mCherry) zebrafish model. Embryos of Tg(FLK-1:mCherry)

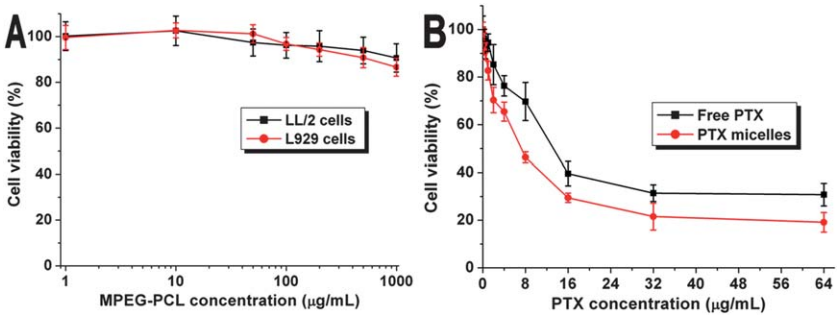

Fig. 4 Cytotoxicity studies of the MPEG-PCL copolymer and the PTX micelles. (A) Cytotoxicity evaluation of the MPEG-PCL copolymer on LL/2 and L929 cells; (B) cytotoxicity studies of the PTX micelles and free PTX on LL/2 cells.

zebrafish were stripped off the egg sheath 48 hpf (Fig. 6B(a and d)), and the bright red fluorescence of blood vessels is shown (Fig. 6B(b and e)). After the injection of free FITC-PTX or FITC-PTX micelles into the zebrafish through the perivitelline space, the FITC-PTX-derived green fluorescence was examined by confocal microscopy in real time. Ten minutes after free FITC-PTX injection, bright green fluorescence could be observed from both the blood vessels and extravascular spaces (Fig. 6B(c)), which indicates that the extravasation of free FITC-PTX from blood to the surrounding tissues was very fast. Regarding the blood vessel extravasation behavior of the FITC-PTX micelles, FITC-PTX-derived green fluorescence was mainly

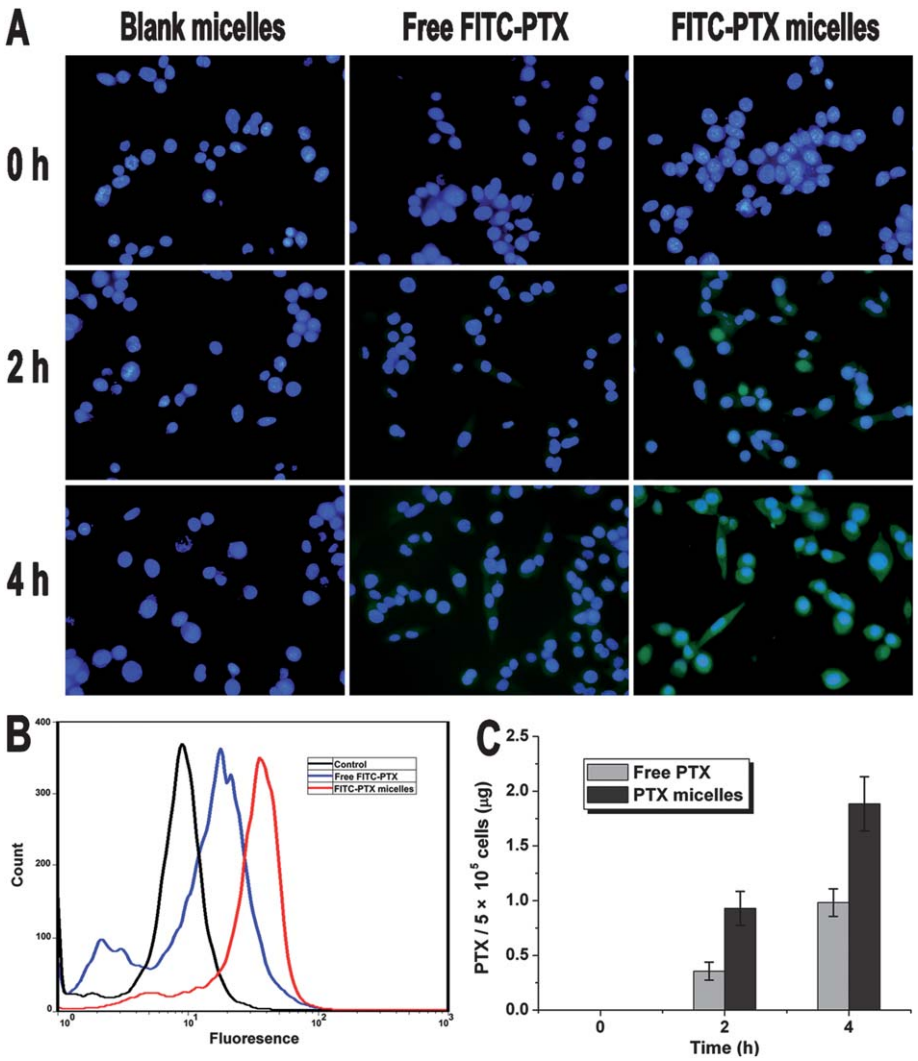

Fig. 5 Cellular uptake of PTX micelles. (A) Fluorescent images of cells treated with medium, blank micelles, free FITC-PTX and FITC-PTX micelles under a confocal microscope at the indicated time intervals. The nuclei were stained blue with DAPI and the cellular distribution of FITC-PTX is shown as green fluorescence in the cytosol. (B) Flow cytometeric histograms for the FITC-PTX micelles on LL/2 cells. (C) PTX accumulation in LL/2 cells.

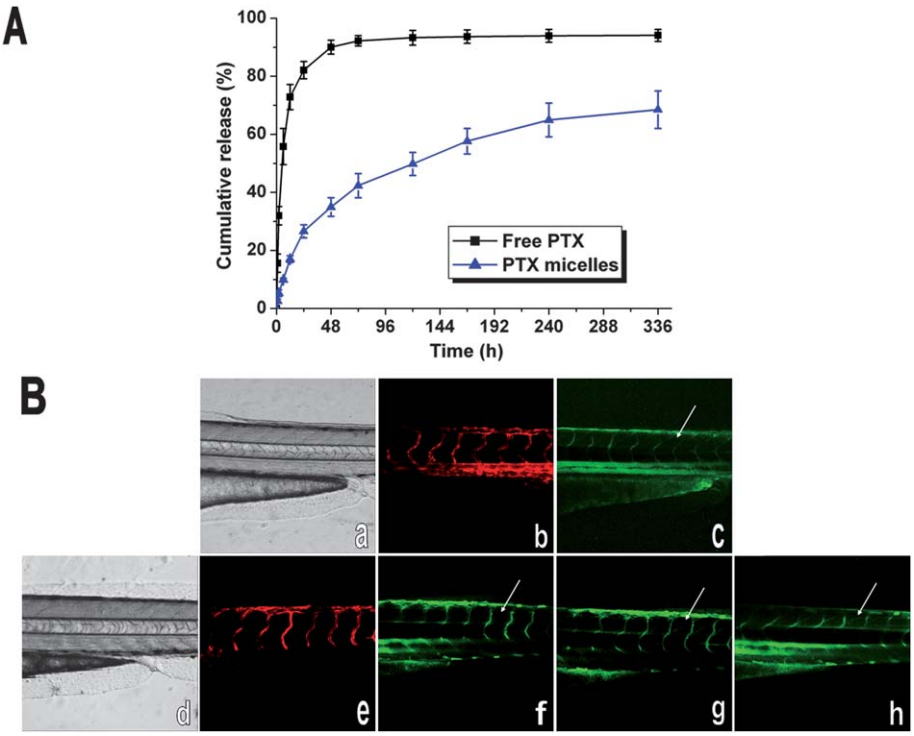

Fig. 6 *In vitro* release behavior and *in vivo* extravasation study of PTX micelles in the transgenic zebrafish model. (A) Drug release profiles of free PTX and PTX micelles in PBS solution at pH 7.4 with error bars representing the standard deviation ($n = 3$); (B) extravasation of free FITC-PTX (a–c) and FITC-PTX micelles (d–h) in the Tg(FLK-1:mCherry) zebrafish model. (a) The brightfield of a zebrafish; (b) the endothelia cell-derived red fluorescence of blood vessels; (c) FITC-PTX-derived green fluorescence 5 min after free FITC-PTX injection; (d) the brightfield of a zebrafish; (e) the endothelia cell-derived red fluorescence of a blood vessel; (f–h) FITC-PTX-derived green fluorescence 10 min, 30 min and 50 min after FITC-PTX micelles injection.

located in the blood vessels and no green fluorescence was observed in the extravascular spaces at 10 minutes after injection, suggesting that FITC-PTX was mainly located in the blood vessels (Fig. 6B(f)). Thirty minutes after injection, a faint green fluorescence was observed in the extravascular spaces, but the fluorescence intensity in the blood vessels was much stronger (Fig. 6B(g)). Fifty minutes after injection, bright green fluorescence was examined in the extravascular spaces (Fig. 6B(h)). From Fig. 6B(f–h), a gradual extravasation behavior of FITC-PTX micelles was observed in real time. The results of this study indicate that encapsulation of PTX in polymeric micelles could decrease the extravasation speed of PTX, which may be because the tightly arranged adjacent endothelial cells of blood vessels could allow the free passage of small molecular PTX, but the PTX micelles with a larger diameter (about 38 nm) may pass through the normal blood vessels only very slowly. The slow extravasation behavior of the FITC-PTX micelles from normal blood vessels may contribute to the enhanced therapeutic effect on tumors and the reduced systemic toxicity of the PTX micelles compared with those of free PTX.

3.5 *In vivo* anti-tumor activity

To compare the anti-tumor effect of the PTX micelles with that of Taxol®, blank micelles and NS, two tumor models were used in this study; the pulmonary metastatic LL/2 model and the subcutaneous LL/2 model. In the pulmonary metastatic LL/2 model, the mean number of tumor nodules (Fig. 7A and C) in the PTX micelles group (18.50 ± 4.04) was dramatically decreased compared with that in the Taxol® (37.67 ± 4.97, $P < 0.001$), blank micelles (80.50 ± 7.20, $P < 0.001$) or NS groups (79.50 ± 6.41, $P < 0.001$). In addition, the weight of the lungs in the PTX micelles group is 0.28 ± 0.02 g (Fig. 7D), *versus* 0.41 ± 0.06 g in the Taxol® group ($P < 0.001$), 0.58 ± 0.04 g in the blank micelles group ($P < 0.001$) and 0.59 ± 0.05 g in the NS group ($P < 0.001$). These findings indicate that the PTX micelles not only inhibited the growth of the implanted tumor, but also impaired tumor metastasis. Furthermore, there was a substantial increase in the life span of the PTX micelles-treated mice; the median survival of the PTX micelles group was 41 days *versus* 32 days, 24 days or 25 days in the Taxol®, blank micelles or NS groups, respectively (Fig. 7B). The body weight of the mice in each group are shown in Fig. 7E, and we found that the body weight in the PTX micelles group is significantly greater than that in the Taxol® group ($P < 0.01$), which implies that the PTX micelles have a lower systemic toxicity compared with Taxol®.

In the subcutaneous LL/2 model (Fig. 8A and C), both Taxol® and the PTX micelles inhibited the growth of tumors ($P < 0.01$), while the blank micelles did not show any anti-tumor activity ($P > 0.05$). Meanwhile, the PTX micelles are more efficient in suppressing growth of tumors compared with the Taxol® group ($P < 0.01$). As shown in Fig. 8B, the weight of tumors in each group also showed that the PTX micelles (1.03 ± 0.16 g) were more effective in the growth inhibition of tumors than the Taxol® (1.93 ± 0.21 g, $P < 0.001$), blank micelles (3.70 ± 0.33 g, $P < 0.001$) or NS groups (3.53 ± 0.36 g, $P < 0.001$). In addition, a survival

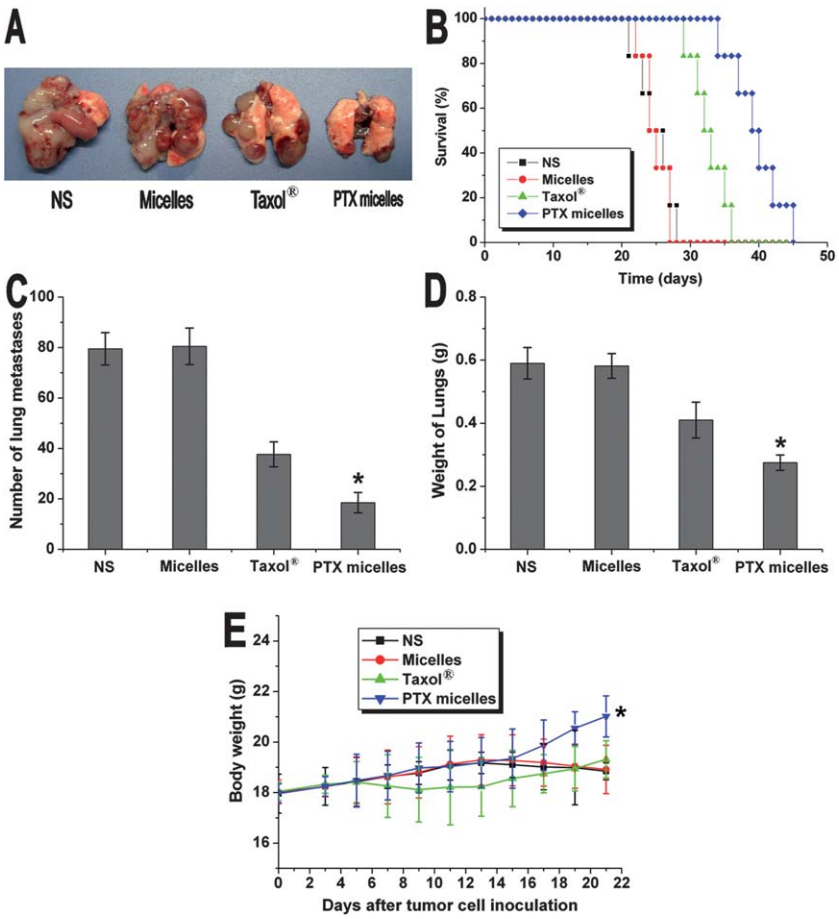

Fig. 7 PTX micelles inhibited growth and metastasis in the pulmonary metastatic LL/2 model. (A) Representative photographs of pulmonary metastatic tumors in each group; (B) survival curve of mice in each group; (C) number of tumor nodules in each group; (D) weight of lungs in each group; (E) body weight in each group.

advantage of the PTX micelles-treated mice was also observed (Fig. 8D). The median survival in the PTX micelles group (47 days) is significantly longer compared with the Taxol® (39 days, $P < 0.01$), blank micelles (32 days, $P < 0.01$) and NS (33 days, $P < 0.01$) groups. Furthermore, the body weight of the mice bearing subcutaneous LL/2 carcinoma in each was monitored. According to Fig. 8E, Taxol® treatment induced a decrease in the body weight of the mice compared with the PTX micelles, which may be due to the severe systemic toxicity caused by Taxol®. The results presented above suggested that PTX micelles were efficient in inhibiting the growth and metastasis of implanted tumors and had a lower systemic toxicity compared with Taxol®.

3.6 Quantitative assessment of apoptosis

We analyzed the effect of the PTX micelles on apoptosis in LL/2 tumors by immunofluorescent TUNEL staining assays. TUNEL positive cells were counted only in regions of intact tumor cell, in which the central necrosis did not interfere with the quantification of apoptosis index. As shown in Fig. 9A–D, within a similar high-power field, more apoptotic cells (with green nuclei) in the tumor tissues were observed in the PTX micelles-treated mice compared with those in the Taxol®, blank micelles or NS groups. The apoptosis index was significantly higher in the PTX micelles group ($9.37 \pm 0.88\%$) than in the Taxol® ($6.78 \pm 0.46\%$, $P < 0.001$), blank micelles ($3.02 \pm 0.46\%$, $P < 0.001$) or NS groups ($2.88 \pm 0.23\%$, $P < 0.001$), respectively (Fig. 9E).

3.7 Determination of tumor cell proliferation

We next examined the proliferation activity of tumor cells by immunohistochemical staining of Ki-67. In Fig. 10A–D, tumors in the Taxol® or PTX micelles groups showed weak Ki-67 immunoreactivity compared with the NS and blank micelles groups and the PTX micelles-treated group showed a more pronounced anti-cell proliferation effect than the Taxol® group. According to Fig. 10E, Ki-67 LI in the PTX micelles-treated group is $23.08 \pm 3.44\%$ *versus* $40.67 \pm 5.12\%$ in the Taxol® group ($P < 0.001$), $71.88 \pm 4.01\%$ in the blank micelles group ($P < 0.001$) and $69.38 \pm 3.15\%$ in the NS group ($P < 0.001$). There was no significant difference between the NS-treated and blank micelles-treated groups ($P > 0.05$).

3.8 Pharmacokinetic and tissue distribution study

The plasma concentration–time profiles of PTX in the PTX micelles and Taxol® group are shown in Fig. 11. After intravenous administration, the peak of plasma concentration (C_{max})

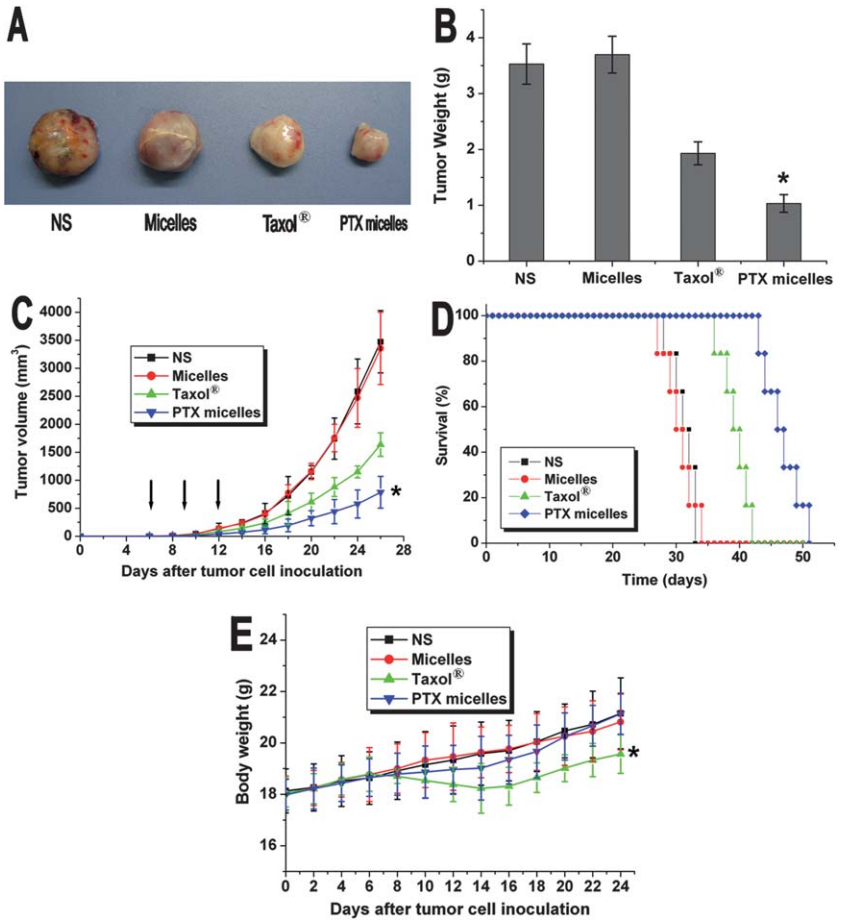

Fig. 8 PTX micelles inhibited growth in subcutaneous LL/2 model. (A) Representative photographs of subcutaneous tumors in each group; (B) weight of subcutaneous tumors in each group; (C) suppression of subcutaneous tumor growth by PTX micelles in mice; (D) survival curve of mice in each group; (E: body weight in each group.

and the time of maximum concentration (T_{max}) were 3.642 ± 0.571 mg L^{-1} and 0.500 ± 0.000 h or 2.856 ± 0.409 mg L^{-1} and 0.600 ± 0.224 h in the PTX micelles or Taxol® groups, respectively. The bioavailability was compared for PTX micelles and Taxol®, which was calculated from the area under the concentration *versus* time curve from 0 to 24 hours (AUC_{0-24}) and the corresponding area under the moment curve ($AUMC_{0-24}$). The AUC_{0-24} and $AUMC_{0-24}$ for PTX micelles was 1.62 times and 3.82 times higher than that for Taxol® (mean = 11.955 ± 1.206 *versus* 7.376 ± 0.580 mg L^{-1} h, difference = 4.579 mg L^{-1} h^{-1}, $P < 0.001$, ANOVA; mean = 69.372 ± 28.014 *versus* 18.164 ± 5.338 mg L^{-1} h^{-2}, difference = 51.208 mg L^{-1} h^{-2}, $P < 0.001$, ANOVA). In addition, the terminal half life ($T_{1/2}$) values for the PTX micelles was 2.30 times higher than that for Taxol® (mean = 9.508 ± 5.313 *versus* 4.130 ± 0.871 h, difference = 5.378 h, $P < 0.001$, ANOVA). After PTX was encapsulated into the micelles, the corresponding total body clearance (CL) decreased from 0.490 ± 0.054 to 0.274 ± 0.069 L h^{-1} kg^{-1}.

Fig. 12 shows the concentration of PTX in the tumor, heart, liver, spleen, lungs and kidneys at different time points after intravenous injection of PTX micelles and Taxol®. After intravenous administration, PTX was distributed into various tissues in 0.5 h. According to Fig. 12, we found that the tissue distribution of the PTX micelles was quite different from that of Taxol®. In tumors, PTX concentrations in the PTX micelles group were significantly higher than those in the Taxol® group at all time points, which may contribute to the EPR effect. Furthermore, in the heart tissue, the PTX concentration in the PTX micelles group was remarkably lower than that in the Taxol® group, whereas, in the liver, the PTX concentration in the PTX micelles group was slightly higher compared with that in the Taxol® group. In other organs (lungs, spleen, and kidneys), no significant differences of PTX concentrations were observed between the PTX micelles and Taxol® groups. These results suggest that after PTX was encapsulated into the MPEG-PCL micelles, the circulation time of PTX in blood was prolonged and the PTX concentration in the tumor site was also increased compared with the commercial formulation Taxol®.

4. Discussion

In our previous work, five MPEG-PCL copolymers and three different methods were used to prepare PTX micelles.[22] Among the MPEG-PCL copolymers, the one with a PEG/PCL ratio of 2000/2000 showed excellent properties in particle size, EE, DL and stability, which is very suitable to prepare PTX micelles. Subsequently, dialysis, solid dispersion, and freeze-drying methods were investigated. For the dialysis method, both the DL

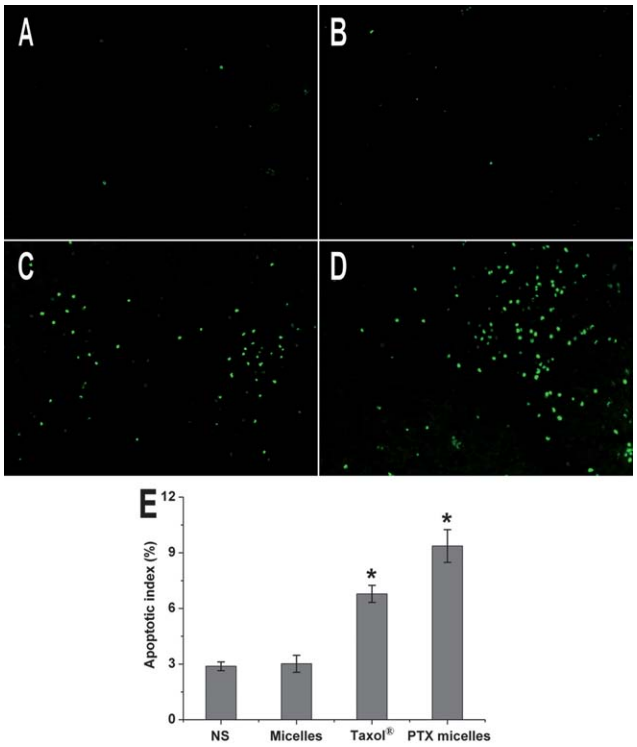

Fig. 9 TUNEL immunofluorescent staining of tumors. (A) Representative TUNEL immunofluorescent images of NS; (B) blank micelles; (C) Taxol® and (D) PTX micelles groups, and (E) mean apoptotic index in each group.

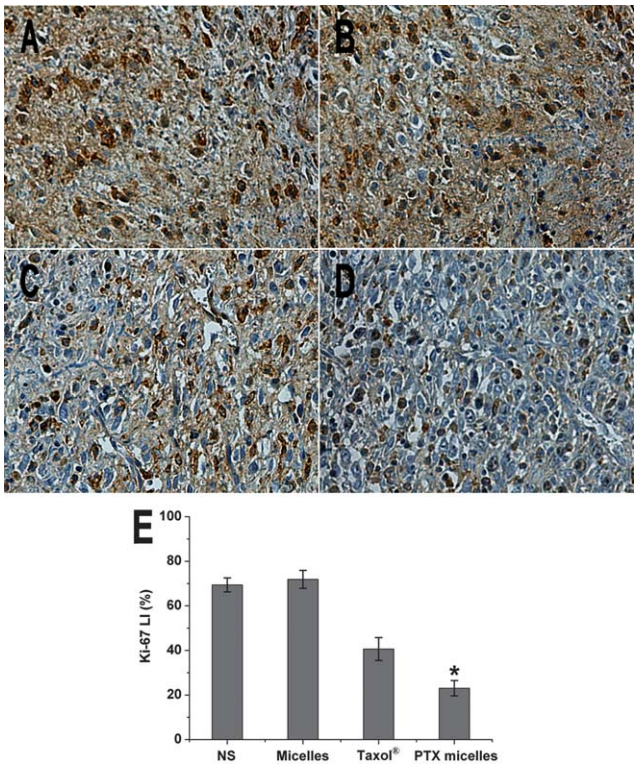

Fig. 10 Ki-67 immunohistochemical staining of tumors. Representative Ki-67 immunohistochemical images of the (A) NS, (B) blank micelles, (C) Taxol® and (D) PTX micelles groups, and (E) mean Ki-67 LI in each group.

and EE of the obtained PTX micelles were disappointing and the recovery rate was very low, which indicated it is not an ideal method for PTX micelles preparation. Compared with the dialysis method, freeze-drying is a simple method with a high DL, EE and recovery rate. However, a poisonous organic solvent, *tert*-butyl alcohol, was used in this procedure, which will limit its applications. For the solid dispersion method, a very high DL, EE and recovery rate could be achieved, and the micelles had a diameter of less than 40 nm. The PTX micelles were prepared in the absence of toxic solvents, surfactants, or cryoprotectors and could be re-dissolved after lyophilization. In addition, the procedure is simple, easy to scale up, and easy to sterilize. The DL of the PTX micelles was up to 25%, but the formed micelles were unstable. Therefore, PTX micelles with a DL of 15% were used in this study.

Several investigations were made in the present study concerning the anti-tumor activity of PTX micelles on pulmonary carcinoma *in vitro* and *in vivo*. We have successfully prepared PTX micelles with high DL, small particle size and sustained release behavior, as demonstrated by our results. The DL and EE of the drug loaded micelles were 14.89% ± 0.06% and 99.25% ± 0.38%, respectively. The average diameter was 38.06 ± 2.30 nm with a PDI of 0.168 ± 0.014 and the particle size and nanostructure were also confirmed by TEM, which suggested the prepared PTX micelles were stable and well-dispersed in aqueous solutions. The findings in cytotoxicity and cellular uptake revealed some properties of the PTX micelles. We found that the PTX micelles showed increased cytotoxicity compared with free PTX, but the MPEG-PCL copolymer exhibited very low toxicity on cells. Subsequently, cellular uptake studies were performed

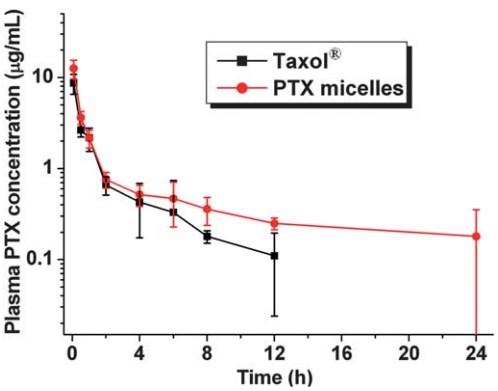

Fig. 11 Plasma concentration–time profiles of PTX after intravenous injection of Taxol® and PTX micelles in mice. Error bars represent the standard deviation ($n = 5$).

using confocal microscopy, FCM and HPLC, respectively. Owing to the absence of fluorescence in PTX, FITC-PTX was synthesised and used in confocal microscopy and FCM analysis. All the results suggested that the higher cytotoxicity of the PTX micelles was associated with their enhanced uptake in cells. Compared with free PTX, the much slower release behavior of PTX from polymeric micelles can be attributed to the "core–shell" structural characteristics of MPEG-PCL micelles as DDS. Furthermore, PTX micelles efficiently suppressed tumor growth and metastasis and prolonged the survival in both the subcutaneous and pulmonary metastatic LL/2 models. The results of

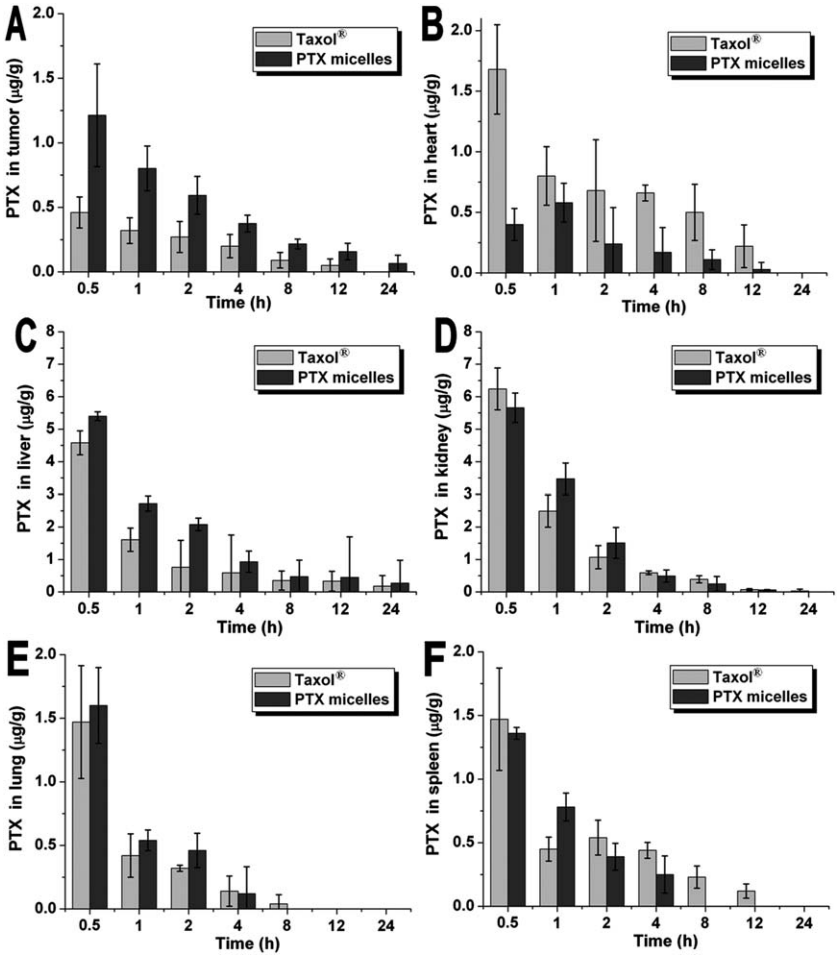

Fig. 12 Tissue distribution of PTX after intravenous injection of Taxol® and PTX micelles in mice. Error bars represent the standard deviation ($n = 5$). Concentration of PTX at different time points in (A) tumor, (B) heart, (C) liver, (D) kidney, (E) lung and (F) spleen, respectively.

TUNEL and Ki67 staining of tumor tissues also confirmed the improved anti-tumor effect of the PTX micelles.

Blood vessels play an essential role in the growth and metastasis of tumors by supplying nutrients and oxygen and removing waste products.[37] Unlike normal blood vessels, gaps between adjacent endothelial cells in tumor blood vessels are very large (200–1200 nm). The defective leaky vascular architecture, as well as poor lymphatic drainage of tumors, induces the EPR effect, which allows nanoscale particles to extravasate into extravascular spaces and accumulate in tumor tissues.[21] To investigate the improved anti-tumor activity of PTX micelles, pharmacokinetic and tissue distribution studies were investigated, which showed that the PTX concentration and the retention time of the PTX micelles in tumors and plasma were significantly higher than those of Taxol®. Therefore, the improved therapeutic effect of the PTX micelles may contribute to the longer circulation time in blood and the accumulation of PTX in tumors by the EPR effect. In addition, the body weight of the PTX micelles-treated mice is significantly higher than that of the Taxol®-treated mice, which implied that the systemic toxicity of the PTX micelles is lower than Taxol® due to the aqueous formulation and sustained release behavior.

A molecular modeling study was employed to investigate the binding affinity between PTX and MPEG-PCL copolymer and the structure of the prepared PTX micelles. The results suggested that PTX could bind with MPEG-PCL copolymer in the PCL segments. Meanwhile, PEG showed a tendency to be more exposed to the solvent (water) than PCL, indicating a core–shell structure of PTX micelles embraced by PEG. These simulations by molecular modeling were consistent with our experimental results. To our knowledge, micelles tend to form aggregates due to their high surface/volume ratio. However, a stable micelles suspension could be obtained through electrostatic interaction and/or a stereospecific blockade of the micelles. In the present work, the prepared PTX micelles are stable with a surface charge of nearly neutral (zeta potential is -1.21 ± 0.44 mV), therefore a stereospecific blockade should contribute to the stability of the PTX micelles. MPEG-PCL is an amphiphilic diblock copolymer consisting of a hydrophobic PCL segment and a hydrophilic PEG segment. The great differences in hydrophobicity between the PCL and PEG segments allow the formation of micelles with a PCL core and a PEG shell. The PEG segments are located at the surface of the micelles and provide limited affinity among the particles to prevent the formation of aggregates.

A conventional formulation of a chemotherapeutic compound showed non-site specificity and extravasated from blood vessels into all the surrounding tissues, inducing severe side effects. Therefore, a decrease of anti-tumor drug extravasation from

normal vessels may reduce their distribution in normal tissues and reduce the systemic toxicity. However, it is difficult to observe the extravasation process of drugs from normal vessels in the existing animal models. In our work, taking the advantages of transparent zebrafish larva and fluorescigenic blood vessels (mCherry-expressed endothelial cells), we used a transgenic zebrafish model to visually observe the extravasation process of FITC-labeled free or micelle-encapsulated PTX in real time. The results showed that entrapping PTX into polymeric micelles reduced the extravasation of PTX from normal blood vessels to the surrounding tissues. The transgenic zebrafish model used in the study is proved to be feasible for *in vivo* drug extravasation studies, and may have potential applications in drug evaluations.

5. Conclusions

In this work, biodegradable polymeric micelles entrapping PTX were prepared and applied to treat LL/2 pulmonary carcinoma *in vitro* and *in vivo*. The obtained PTX micelles showed increased cellular uptake, enhanced cytotoxicity, sustained *in vitro* release behavior and slow extravasation from blood vessels in the transgenic zebrafish model. The PTX micelles were more effective in suppressing tumor growth and metastases and enabled prolonged survival in the LL/2 tumor model compared with Taxol®. Encapsulation of PTX in polymeric micelles altered the pharmacokinetics and increased the PTX concentration in tumors. Therefore, the prepared PTX micelles are an excellent aqueous formulation of PTX for intravenous application with improved anti-tumor activity and lower toxicity, which may serve as a candidate for pulmonary carcinoma therapy.

References

1 R. Siegel, D. Naishadham and A. Jemal, *Ca-Cancer J. Clin.*, 2012, **62**, 10–29.
2 R. F. Ozols, M. A. Bookman and R. C. Young, *N. Engl. J. Med.*, 2006, **354**, 1641–1643.
3 D. Elias, F. Blot, A. El Otmany, S. Antoun, P. Lasser, V. Boige, P. Rougier and M. Ducreux, *Cancer*, 2001, **92**, 71–76.
4 A. G. Portilla, P. H. Sugarbaker and D. Chang, *World J. Surg.*, 1999, **23**, 23–29.
5 P. H. Sugarbaker and K. A. Jablonski, *Ann. Surg.*, 1995, **221**, 124.
6 D. Armstrong, B. Bundy, L. Wenzel, H. Huang, R. Baergen, S. Lele, L. Copeland, J. Walker and R. Burger, *N. Engl. J. Med.*, 2006, **354**, 34–43.
7 T. M. Allen and P. R. Cullis, *Science*, 2004, **303**, 1818–1822.
8 C. Gong, X. Wei, X. Wang, Y. Wang, G. Guo, Y. Mao, F. Luo and Z. Qian, *Nanotechnology*, 2010, **21**, 215103.
9 C. Y. Gong, S. Shi, X. H. Wang, Y. J. Wang, S. Z. Fu, P. W. Dong, L. J. Chen, X. Zhao, Y. Q. Wei and Z. Y. Qian, *J. Phys. Chem. B*, 2009, **113**, 10183–10188.
10 A. J. J. Wood, E. K. Rowinsky and R. C. Donehower, *N. Engl. J. Med.*, 1995, **332**, 1004–1014.
11 D. M. Vyas and F. Vittorio, in *Pharmacochemistry Library*, Elsevier, 1995, vol. 22, pp. 103–130.
12 R. B. Weiss, R. Donehower, P. Wiernik, T. Ohnuma, R. Gralla, D. Trump, J. Baker Jr, D. Van Echo, D. Von Hoff and B. Leyland-Jones, *J. Clin. Oncol.*, 1990, **8**, 1263–1268.
13 E. Rowinsky, E. Eisenhauer, V. Chaudhry, S. Arbuck and R. Donehower, *Semin. Oncol.*, 1993, **20**, 1–15.
14 V. Wagner, A. Dullaart, A.-K. Bock and A. Zweck, *Nat. Biotechnol.*, 2006, **24**, 1211–1217.
15 R. K. Jain and T. Stylianopoulos, *Nat. Rev. Clin. Oncol.*, 2010, **7**, 653–664.
16 B. Y. S. Kim, J. T. Rutka and W. C. W. Chan, *N. Engl. J. Med.*, 2010, **363**, 2434–2443.
17 O. C. Farokhzad, J. Cheng, B. A. Teply, I. Sherifi, S. Jon, P. W. Kantoff, J. P. Richie and R. Langer, *Proc. Natl. Acad. Sci. U. S. A.*, 2006, **103**, 6315–6320.
18 K. L. Hennenfent and R. Govindan, *Ann. Oncol.*, 2006, **17**, 735–749.
19 C. Oerlemans, W. Bult, M. Bos, G. Storm, J. F. W. Nijsen and W. E. Hennink, *Pharm. Res.*, 2010, **27**, 2569–2589.
20 M. Yokoyama, *Expert Opin. Drug Delivery*, 2010, **7**, 145–158.
21 J. Fang, H. Nakamura and H. Maeda, *Adv. Drug Delivery Rev.*, 2011, **63**, 136–151.
22 C. Wang, Y. J. Wang, M. Fan, F. Luo and Z. Y. Qian, *Int. J. Pharm.*, 2011, **414**, 251–259.
23 C. Y. Gong, S. Shi, P. W. Dong, B. Kan, M. L. Gou, X. H. Wang, X. Y. Li, F. Luo, X. Zhao, Y. Q. Wei and Z. Y. Qian, *Int. J. Pharm.*, 2009, **365**, 89–99.
24 C. Y. Gong, Y. J. Wang, X. H. Wang, X. W. Wei, Q. J. Wu, B. L. Wang, P. W. Dong, L. J. Chen, F. Luo and Z. Y. Qian, *J. Nanopart. Res.*, 2010, **13**, 721–731.
25 C.-Y. Gong, S. Shi, X.-Y. Peng, B. Kan, L. Yang, M.-J. Huang, F. Luo, X. Zhao, Y.-Q. Wei and Z.-Y. Qian, *Growth Factors*, 2009, **27**, 377–383.
26 M. L. Rodrigues, P. Carter, C. Wirth, S. Mullins, A. Lee and B. K. Blackburn, *Chem. Biol.*, 1995, **2**, 223–227.
27 H. HyperChem Professional 8.0, Inc., 1115 NW 4th Street, Gainesville, Florida 32601, USA.
28 W. L. Jorgensen, D. S. Maxwell and J. Tirado-Rives, *J. Am. Chem. Soc.*, 1996, **118**, 11225–11236.
29 R. Fletcher and C. Reeves, *Comput. J.*, 1964, **7**, 149–154.
30 N. Foloppe and A. D. MacKerell Jr, *J. Comput. Chem.*, 2000, **21**, 86–104.
31 C. Zhao, X. Wang, Y. Zhao, Z. Li, S. Lin, Y. Wei and H. Yang, *PLoS One*, 2011, **6**, e21768.
32 C. Zhao, H. Yang, H. Shi, X. Wang, X. Chen, Y. Yuan, S. Lin and Y. Wei, *Carcinogenesis*, 2011, **32**, 1143–1150.
33 M. Westerfield, *The Zebrafish Book: A Guide for the Laboratory Use of Zebrafish (*Brachydanio Rerio*)*, University of Oregon Press Eugene, OR, 1993.
34 S. A. Ben-Sasson, Y. Sherman and Y. Gavrieli, *Methods Cell Biol.*, 1995, **46**, 29–39.
35 J. Halder, A. A. Kamat, C. N. Landen Jr, L. Y. Han, S. K. Lutgendorf, Y. G. Lin, W. M. Merritt, N. B. Jennings, A. Chavez-Reyes, R. L. Coleman, D. M. Gershenson, R. Schmandt, S. W. Cole, G. Lopez-Berestein and A. K. Sood, *Clin. Cancer Res.*, 2006, **12**, 4916–4924.
36 O. Trott and A. J. Olson, *J. Comput. Chem.*, 2010, **31**, 455–461.
37 P. Carmeliet and R. K. Jain, *Nature*, 2011, **473**, 298–307.